Journal of Power Sources 300 (2015) 351–357

Contents lists available at ScienceDirect

Journal of Power Sources

journal homepage: www.elsevier.com/locate/jpowsour

Double locked silver-coated silicon nanoparticle/graphene core/shell fiber for high-performance lithium-ion battery anodes

Minsu Gu [a, 1], Seunghee Ko [a, 1], Seungmin Yoo [a, b, 1], Eunhee Lee [a], Sa Hoon Min [a], Soojin Park [a, **], Byeong-Su Kim [a, c, *]

[a] Department of Energy Engineering, School of Energy and Chemical Engineering, Ulsan National Institute of Science and Technology (UNIST), Ulsan 689-798, Republic of Korea
[b] Department of Environmental and Chemical Industry, Ulsan College, Ulsan 680-749, Republic of Korea
[c] Department of Chemistry, School of Natural Science, Ulsan National Institute of Science and Technology (UNIST), Ulsan 689-798, Republic of Korea

HIGHLIGHTS

- Core/shell structured graphene fiber with silver-coated silicon was formed by wet-spinning.
- This study examined the battery performance depending on structural effect and different reduction conditions.
- We achieved a highly enhanced performance of capacity and excellent rate capabilities, comparing to simple mixture.

GRAPHICAL ABSTRACT

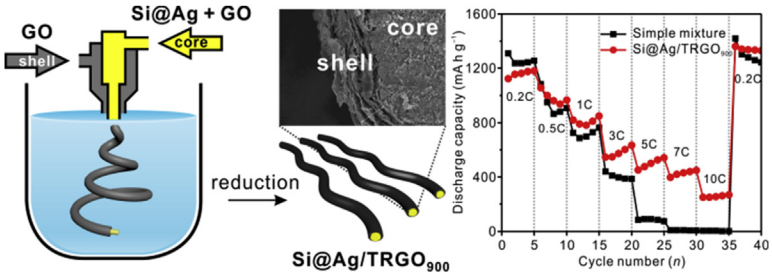

ARTICLE INFO

Article history:
Received 25 June 2015
Received in revised form
10 September 2015
Accepted 22 September 2015
Available online xxx

Keywords:
Wet-spinning
Core/shell fiber
Graphene oxide
Silicon anode
Lithium-ion batteries

ABSTRACT

We present a fabrication of scalable coaxial core/shell silicon (Si)-graphene fiber prepared by dual-nozzle-induced wet-spinning assembly for high-performance Si anode. Over 50 wt% of Si nanoparticles mixed with graphene oxide suspension can be incorporated in the core with the outstanding dispersibility of unique silver-coated Si nanoparticles in aqueous media. The core fiber is further encapsulated by graphene shell which not only provides conducting pathways, but also alleviates severe volume expansion of Si core. This novel core/shell Si anode with double locked graphene architecture delivers more stable cycle performance and superior rate capability than anodes composed of simple mixture of Si-graphene composites.

© 2015 Elsevier B.V. All rights reserved.

1. Introduction

Lithium-ion batteries (LIBs) have been intensively developed as one of the most promising energy storage devices. The potential uses of LIBs to power future portable electronic devices, electrical vehicles, and smart grids have prompted the development of novel materials and systems to enhance the energy density and cycle life of LIBs [1,2]. However, conventional graphite anodes with a low

* Corresponding author. Department of Energy Engineering, School of Energy and Chemical Engineering, Ulsan National Institute of Science and Technology (UNIST), Ulsan 689-798, Republic of Korea
** Corresponding author.
E-mail addresses: spark@unist.ac.kr (S. Park), bskim19@unist.ac.kr (B.-S. Kim).
[1] These authors contributed equally to this work.

http://dx.doi.org/10.1016/j.jpowsour.2015.09.083
0378-7753/© 2015 Elsevier B.V. All rights reserved.

theoretical capacity (372 mA h g^{-1}) in LIBs cannot meet the demand for high power and energy density for future advanced devices and large-scale energy storage systems.

As an alternative, silicon (Si) has received considerable attention recently as a next-generation anode material because of its highest theoretical specific capacity of *ca.* 3500 mA h g^{-1} as well as low lithiation potential, low cost, and environmental safety [3–5]. Despite these favorable features, commercialization of Si-based anodes is still not realized owing to their low intrinsic electrical conductivity and significant challenges such as a considerable volume change (>300%) during the lithiation–delithiation process and safety issues related to lithiated Si. In particular, the volume change causes high stress and pulverization, and eventually breaks down the electrical contact from the current collector or other conductive phases, resulting in degradation of the electrode and a limited cycle life [6–8]. Therefore, extensive research efforts have endeavored to alleviate the aforementioned challenges, and thereby to improve the electrochemical performance of Si-based anode materials.

Nanostructured Si anode materials with various morphologies such as nanoparticles, nanotubes, nanowires, and thin films have been developed to overcome the problem of volume change, and to improve cycle performance [9–11]. These nanostructured Si anodes offer potential solutions by providing a smaller absolute volume change, as well as additional benefit of the short diffusion path of the Li^+ ion that enhances kinetic performance. However, there are problems associated with the intrinsic nanoscale dimensions of these anodes: their large surface areas and low packing density are responsible for serious side reactions with the electrolyte and low volumetric energy density, respectively. Thus, Si composites with carbon supporting materials (e.g., carbon black and carbon nanotubes) have exploited to realize considerably enhanced cell performance: the outstanding multi-functionality of the composites enables protection of the Si surface from electrolyte and imparts superior conductive properties and mechanical flexibility that is sufficient to alleviate extensive volume expansion [12,13].

Among various carbon supporting materials, in particular, graphene and its derivatives have been actively employed owing to their superior electrical, thermal, and mechanical strength. For example, there have been reports of synthesizing composites of Si and graphene by a number of different methods, including electrostatic attraction [14–16], freeze-drying [17], vacuum filtration [18–20], ultrasonication [21], cross-linking [22,23], plasma-assisted ball-milling [24,25], electrospinning [26,27], and layer-by-layer assembly [28,29]. These approaches demonstrate that graphene acts as an elastic buffer to accommodate the volume expansion of Si nanoparticles and as a good electron conductor. However, it is still highly desirable to develop a simple, scalable, and effective strategy that can utilize the strength of carbon materials such as graphene to overcome the limitations of Si anodes.

Herein, we developed a large-scale solution-processable fabrication method to produce core/shell structured graphene fiber with silver-coated Si (Si@Ag) nanoparticles for high performance anodes by a dual-nozzle wet-spinning assembly strategy (Scheme 1). Si@Ag nanoparticles were used to provide outstanding conductivity and improved cycle life as demonstrated in our previous report [30]. We further examined the architectural effect of core/shell structures by comparing the performance between coaxial core/shell fibers and simple mixtures. The coaxial fibers showed highly improved electrochemical performance not only with high charge–discharge capacities, but also with excellent rate capabilities even at a high rate of 10C due to the improved mechanical strength and electron pathway between Si nanoparticles and graphene sheets. Finally, we demonstrated that the uniquely interconnected core/shell structure exhibited electrical conductivity without any conducting agents such as super P carbon black.

2. Experimental

2.1. Synthesis of Si@Ag nanoparticles

The Si@Ag nanoparticles were prepared according to previous literature [30]. In brief, 0.25 g of Si powder (average diameter of 50 nm, 99.9%, Aldrich) was dispersed into 20 mL of ethanol at 50 °C in a propylene reactor. Subsequently, 5.0 mM of silver nitrate ($AgNO_3$, Aldrich) and 5.0 mM of *n*-butylamine (Aldrich) was added to the solution with stirring for 10 min. As-synthesized Si@Ag nanoparticles were rinsed with ethanol to remove excess Ag precursor. Finally, it was filtered out and dried at 80 °C for 12 h in a vacuum oven.

2.2. Synthesis of graphene oxide suspension

Graphite oxide was synthesized from graphite powder by modified Hummers method and exfoliated to give a brown dispersion of graphene oxide (GO) under ultrasonication [31,32].

2.3. Preparation of core/shell structured Si@Ag/GO fibers by wet-spinning

Core/shell structured Si@Ag/GO fibers were fabricated by wet-spinning method using dual-nozzle. Si@Ag nanoparticles dissolved in deionized water (200 mg/mL) were mixed with GO dispersion (20 mg/mL) (Si@Ag:GO = 1:1, v/v) to enhance the conductivity among Si@Ag nanoparticles. This homogenously mixed solution was transferred to a syringe which is connected to the core channel of spinneret, while the separate GO dispersion (20 mg/mL) was connected to the shell channel of spinneret. The core (at a rate of 10 mL/h) and shell (at a rate of 60 mL/h) solutions are injected to coagulation solution containing chitosan solution (0.50 wt% in 0.50 wt% acetic acid). After immersion for 30 min in a coagulation bath, the as-prepared Si@Ag/GO fibers were dipped into 0.50 wt% acetic acid for 3 h and then finally washed with deionized water for 3 h to remove the residual coagulation solution. The washed Si@Ag/GO fibers were collected by vacuum filtration.

2.4. Reduction of Si@Ag/GO fibers

The chemical reduction of the Si@Ag/GO fibers was typically carried out with a hydrazine vapor treatment at 80 °C for 24 h to afford chemically reduced Si@Ag/GO fibers (hereafter, Si@Ag/CRGO). The thermal reduction was further performed by heating the sample in a quartz furnace under an argon atmosphere. The temperature was raised to 200 or 900 °C at a rate of 5 °C/min, maintained for 1 h, and slowly cooled down to room temperature to provide thermally reduced Si@Ag/CRGO fibers of Si@Ag/$TRGO_{200}$ and Si@Ag/$TRGO_{900}$, respectively.

2.5. Characterizations

Inductively coupled plasma-mass spectrometer (ICP-MS; Perkin Elmer, ELAN DRC-II) analysis was used to confirm the content of Ag on the Si nanoparticles. Field emission scanning electron microscopy (FE-SEM; Hitachi, S-4800) was used to observe surface morphologies of wet-spun samples. Thermogravimetric analysis (TGA; TA instruments, Q50) was used to calculate the mass content of Si and GO. The microstructures of samples were studied using a high power X-ray diffractometer (XRD) and a Cu Kα source (Rigaku, D/MAZX 2500V/PC).

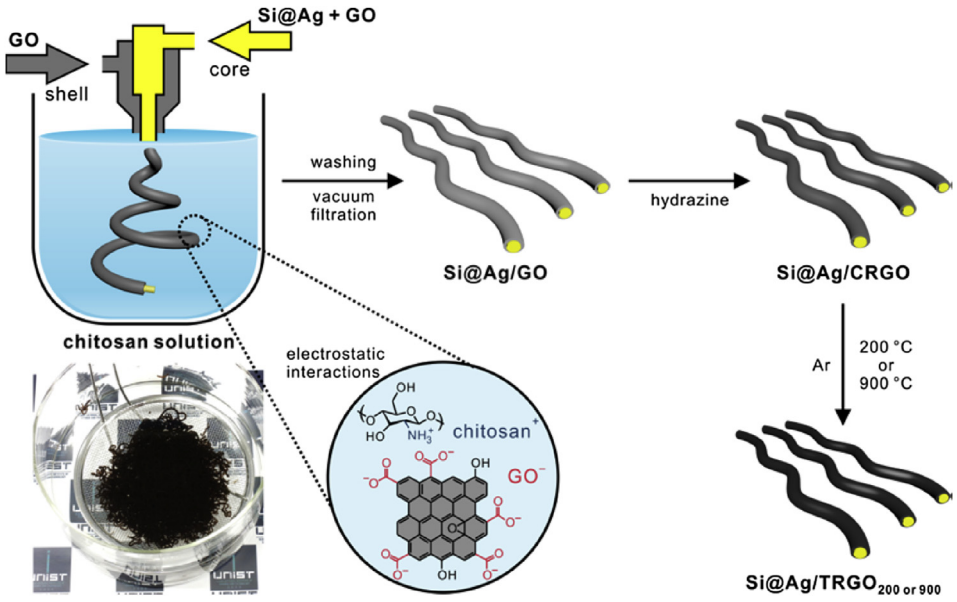

Scheme 1. Schematic illustration of coaxial Ag coated Si–graphene fibers by wet-spinning process.

2.6. Electrochemical analysis

The electrochemical properties of simple mixture and coaxial fiber electrodes were tested by galvanostatic discharging and charging processes in coin-type half cells (2016 R-type) with 20 mm in diameter and 1.6 mm in thickness. The cells were composed of active material/super P carbon black/binder composite as a working electrode and lithium metal as a counter electrode, and prepared in an argon-filled glove box. The electrode consisting of active material (simple mixture or coaxial fiber, 80 wt %), super P carbon black (conducting agent, 10 wt%, TIMCAL), and poly(acrylic acid)/sodium carboxymethyl cellulose (50/50, wt/wt, Aldrich) binder (10 wt%) with active mass loading amount of ~1 mg/cm^2. The resulting slurry was coated on a copper current collector and dried in a vacuum oven at 150 °C for 2 h. The electrolyte was composed of 1.3 M $LiPF_6$ in ethylene carbonate/diethyl carbonate (EC/DEC, 30/70 v/v, Panaxetec) with 10 wt% fluoroethylene carbonate (FEC). The cells were cycled at a rate of 0.05–10C between 0.005 and 1.5 V (vs. Li/Li$^+$). All the electrochemical measurements were carried out with a WBCS-3000 battery cycler (Wonatech Co.) at room temperature. Electrochemical impedance spectroscopy (EIS) measurements were performed in the frequency range from 10 mHz to 1 MHz with an amplitude of 10 mV at the charged state (~1.5 V).

3. Results and discussion

We introduced a dual-nozzle wet-spinning method to fabricate the core/shell-structured fibers using the Si@Ag nanoparticle solution for the core and the GO suspension for the shell nozzle (Scheme 1). Electrically conductive Si@Ag nanoparticles were initially synthesized by the chemical reduction of Ag$^+$ ions in the presence of Si nanoparticles with a mild reducing agent, as reported in our previous paper [30]. This method provides the formation of Ag nanoparticles coated on the Si nanoparticles in an aqueous solution with an average diameter of 13 nm for Ag nanoparticles on 50 nm Si nanoparticles (see Figure S1 in Supplementary data). The content of Ag nanoparticles was ~3 wt% as confirmed by inductively coupled plasma-mass spectrometer (ICP-MS) analysis. Owing to their good dispersion in aqueous solution, Si@Ag nanoparticles are compatible with the stable GO suspension prepared using the modified Hummers method [31,32]. The coaxial Si@Ag/GO fibers were produced by coagulation in a chitosan solution through polyionic complexation between negatively charged GO sheets and positively charged chitosan solution [33]. The as-prepared core/shell Si@Ag/GO fibers exhibit mechanical stability due to the electrostatic interaction between chitosan and GO. The robust mechanical properties of coaxial fibers were also demonstrated by winding fibers with lengths of several tens of centimeters long around a glass rod (see Figure S2 in Supplementary data). It is also important to note that this method is highly scalable for mass production of graphene based composites, benefiting from the solution-processable wet-spinning method.

The scanning electron microscopy (SEM) image in Fig. 1a shows the successful enveloping of Si@Ag nanoparticles by the GO shells. The diameter of the Si@Ag/GO fibers is about 380 μm, including 270 μm diameter of the Si@Ag core fibers. Once the coaxial fiber was produced, Si@Ag/GO underwent a reduction process by chemical and thermal protocols to enhance the electrical conductivity and the integrity of the resulting composite. As shown in Fig. 1b, c and S3, the diameter of Si@Ag/GO fibers decreased after the reduction process to 360 μm, including 233 ± 23.5 μm diameter of the core of Si@Ag fibers, and the shell thickness of the fibers was ranged from 15 to 65 μm with an average thickness of 39.1 μm. The magnified SEM image of core Si@Ag fibers revealed that Si@Ag nanoparticles were uniformly confined and well interconnected with graphene sheets within the core (Fig. 1d). The graphene sheets within the Si core fiber can play a critical role of enhancing the electrical conductivity and further reinforcing the mechanical strength of the Si core fiber together with the additional graphene shell. As a result, the double locked graphene structure of the coaxial fiber can accommodate a large volume change of the Si nanoparticles and facilitate the electron conduction from Li$^+$ ions during the lithiation–delithiation process, by enhancing the interconnection between Si@Ag nanoparticles and graphene sheets in the core fiber and encapsulating the Si core fiber with the graphene shell.

Thermogravimetric analysis (TGA) was used to classify each contribution of Si and graphene in Si@Ag/$TRGO_{900}$ fibers in 60% O_2 and 40% N_2 condition. Si@Ag/$TRGO_{900}$ fibers showed decom-

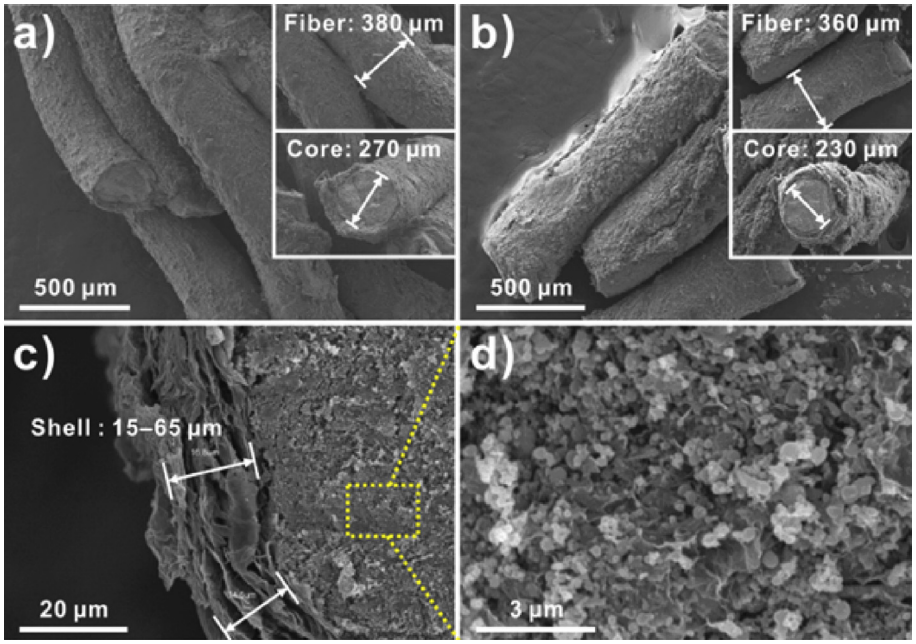

Fig. 1. SEM images of (a) as-prepared Si@Ag/GO fibers and (b–d) the Si@Ag/TRGO$_{900}$ fibers after chemical and thermal reduction. (d) Magnified SEM image of internal structure of the core fiber in part c.

position at 500 °C by degradation of graphene, remaining the amount of about 57% and mass fraction was subsequently increased above 500 °C due to the oxidation of containing Si@Ag nanoparticles in core fibers (Fig. 2a). In order to confirm the compositional ratio in Si@Ag/TRGO$_{900}$, the individual Si@Ag nanoparticles and TRGO$_{900}$ fibers were also analyzed because each content can be calculated by a simple Equation (1) [14].

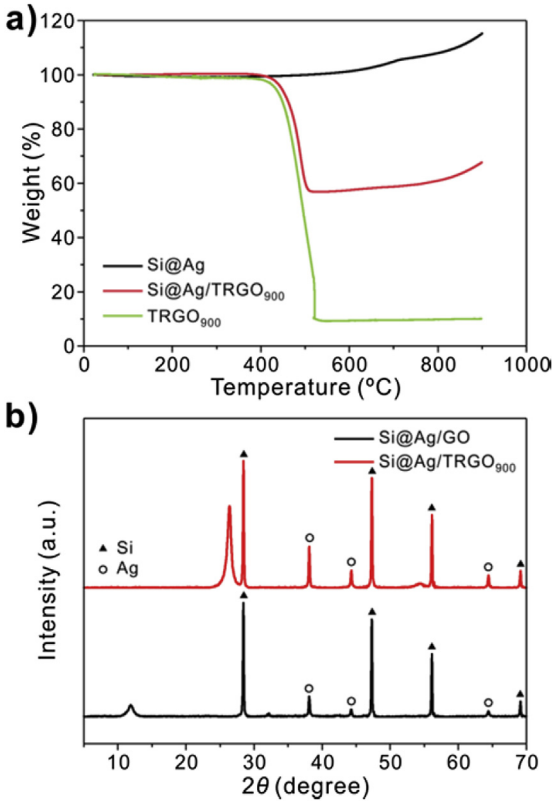

Fig. 2. (a) TGA of Si@Ag nanoparticles, Si@Ag/TRGO$_{900}$, and TRGO$_{900}$ fibers in 60% O_2 and 40% N_2 condition at a rate of 5 °C/min. (b) XRD of Si@Ag/GO and Si@Ag/TRGO$_{900}$ fibers with characteristic diffraction patterns of Si and Ag.

$$W_{Si@Ag}X_{Si@Ag} + W_{TRGO900}(1 - X_{Si@Ag}) = W_{Si@Ag/TRGO900} \quad (1)$$

where $W_{Si@Ag}$, $W_{TRGO900}$, and $W_{Si@Ag/TRGO900}$ are residual weight percent of Si@Ag, TRGO$_{900}$, and the Si@Ag/TRGO$_{900}$ fibers, respectively. $X_{Si@Ag}$ is the Si@Ag content in the Si@Ag/TRGO$_{900}$ fibers. Si@Ag was partially oxidized above 500 °C in O_2 condition of TGA with a increase in mass (~115%). TRGO$_{900}$ fibers without Si@Ag did not show any increment above 500 °C with remaining 9% resultant. As a result, Si@Ag/TRGO$_{900}$ fibers contained approximately 48 wt% TRGO$_{900}$ and 52 wt% Si@Ag, respectively, without any residues. It shows that over 50 wt% of Si nanoparticles mixed with GO sheets were incorporated in the core because of the outstanding compatibility of aqueous Si@Ag nanoparticles with the stable GO suspension.

We could also confirm the degree of reduction of Si@Ag/GO as different reduction process through TGA. In the case of Si@Ag/GO fibers, many oxygen-containing functional groups of GO such as carboxyl, hydroxyl, and epoxide groups accounting for about 36 wt % were mainly decomposed at 200 °C (see Figure S4 in Supplementary data). Some portion of oxygen-containing functional groups disappeared after hydrazine vapor reduction, but still remained (~16 wt%) in the 25–400 °C range of Si@Ag/CRGO fibers, while Si@Ag/TRGO$_{900}$ fibers did not show any decomposition of functional groups, indicating Si@Ag/GO fibers was entirely reduced. It means that additional thermal reduction is necessary for inhibiting the side reaction between functional groups and electrolyte as well as enhanced conductivity of fully reduced GO.

The successful reduction of the graphene fiber is also supported by X-ray diffraction (XRD) analysis as presented in Fig. 2b. After reduction, the broad XRD peak of GO at 11.9° disappeared and the new peak at 26.4° appeared, corresponding to the *d*-spacing of 0.338 nm which is close to that of natural graphite (0.335 nm), while Si@Ag/TRGO$_{900}$ showed no significant change in the XRD

characteristic peaks of Si and Ag.

In order to investigate the effect of the architecture of double locked graphene on the Si nanoparticles, electrochemical properties of Si@Ag/TRGO$_{900}$ and simple mixture of Si@Ag and TRGO$_{900}$ as the anodes in LIBs were evaluated using a coin-type half cell (2016R) within 0.005–1.5 V (vs. Li/Li$^+$). All samples were fabricated using the same composition. Simple mixed sample was physically mixed with two components, while Si@Ag/TRGO$_{900}$ was obtained by the wet-spinning process that enables graphene to be applied both in the core and shell of the coaxial fibers.

Fig. 3 and S5 compare electrochemical performance for simple mixture and Si@Ag/GO fibers treated by different reduction processes. Si@Ag/TRGO$_{900}$ exhibited a relatively low discharge (charge) capacities of 1423 mA h g^{-1} (1124 mA h g^{-1}) with coulombic efficiency of 79.0% compared to simple mixed composite, 1603 mA h g^{-1} (1309 mA h g^{-1}) with coulombic efficiency of 81.7%, at first cycle at 0.05C rate (Fig. 3a). It is obvious that Si@Ag/TRGO$_{900}$ showed a better cycling performance with a charge capacity of 974 mA h g^{-1} after 100 cycles at 0.2C rate, corresponding to 86.7% capacity retention, while simple mixture showed the specific charge capacity of 959 mA h g^{-1} after 100 cycles, corresponding to capacity retention of 73.3% through a normalized capacity by dividing the first charge capacity (Fig. 3b). It is expected that the active Si materials in the simple mixture react more easily with Li ions by their large surface area exposed to the electrolyte, resulting in the high capacity at the first cycle. The cell with simple mixture, however, suffered from the severe capacity drop at initial few cycles due to the loss of active materials by significant structure destruction during continuous cycling. On the contrary, the cell with doubly protected Si@Ag/TRGO$_{900}$ displayed stable cycle retention without a noticeable decline in capacity, in spite of the low capacity at the first cycle for the hindrance of Li ion diffusion by graphene [20,34,35].

Especially, the rate performance of Si@Ag/TRGO$_{900}$ was superior to that of the simple mixture. The rate capabilities of both electrodes are plotted in Fig. 3c. The improved electrochemical performances can be explained as follows: (i) the dual graphene-protected core/shell structure plays a key role in alleviating the mechanical stress on the Si nanoparticles during large volume change in cycling; and (ii) the uniform dispersion of Si nanoparticles in graphene layers in core fiber leads to a significant enhancement in the electrical conductivity of Si nanoparticles with the highly improved electron pathway than that of simple mixed sample.

Reduction process has strongly affected the cell performance in Si@Ag/GO. Both Si@Ag/CRGO and Si@Ag/TRGO$_{200}$ showed lower charge capacity and coulombic efficiency than Si@Ag/TRGO$_{900}$ and simple mixture with TRGO$_{900}$, which was completely reduced with enhanced electrical conductivity as shown in Fig. 3a. This may be attributed to the functional groups that remained on the graphene fiber surface, and it can cause serious side reactions during the lithiation process in carbonate-based electrolytes [36]. Even though all samples were fabricated via a wet-spinning process, the graphene layers irrespective of the position of the fibers were different depending on the reduction processes. Generally, poor electrochemical performance was observed when CRGO was used as the anode in LIBs. However, the CRGO subjected to additional thermal reduction at high temperature showed much higher specific capacity, because functional groups on the GO surface was removed completely as confirmed by TGA analysis [34,37,38]. As a result, the side reaction of the Si@Ag/TRGO$_{900}$ was significantly decreased compared to that of other samples with much higher specific capacity and coulombic efficiency.

To verify excellent cycling and rate performances of Si@Ag/TRGO$_{900}$ fibers, the electrochemical impedance spectroscopy (EIS) measurements of the simple mixture and the Si@Ag/TRGO$_{900}$ were also performed on cycled (first and 50th) electrodes (Fig. 4). According to the equivalent circuit, R_S is the ohmic series resistance that is associated with the cell components, such as the electrolyte or other components. R_{SEI} is the Li ion transfer resistance through the SEI layer, R_{CT} is the charge transfer resistance, and W is the Warburg impedance about the Li ion diffusion into the active materials. The capacitor components were replaced by the constant phase elements (CPE$_1$ and CPE$_2$). In the EIS spectra, the total cell resistance of the simple mixture and the Si@Ag/TRGO$_{900}$ were 88 and 78 Ω after the first cycle, respectively. After 50th cycles, the total resistance of the simple mixture was 122 Ω, while that of the Si@Ag/TRGO$_{900}$ was 102 Ω. Although the values of both electrodes increased after 50th cycles, the total resistance in the core/shell structured Si@Ag/TRGO$_{900}$ increased less than that in the simple mixture. It is attributed that the double locked graphene layers enhance the structural integrity and electrical conductivity of the Si@Ag/TRGO$_{900}$ electrodes during charge and discharge cycles. Another noticeable point is that most of surfaces of the electrodes consisting of Si and graphene were covered with SEI layers after long cycling. As the electrode was fabricated with a mixture of conducting agent and binder, it was hard to discern the architecture of coaxial fibers; nonetheless, we found that the overall electrode structure did not undergo severe volume changes causing deterioration of cycling performance (see Figure S6 in Supplementary Information).

Furthermore, we investigated electrochemical properties of Si@Ag/TRGO$_{900}$ electrodes without a conducting agent (Fig. 5). In most of LIBs, the conducting agent has been used to facilitate

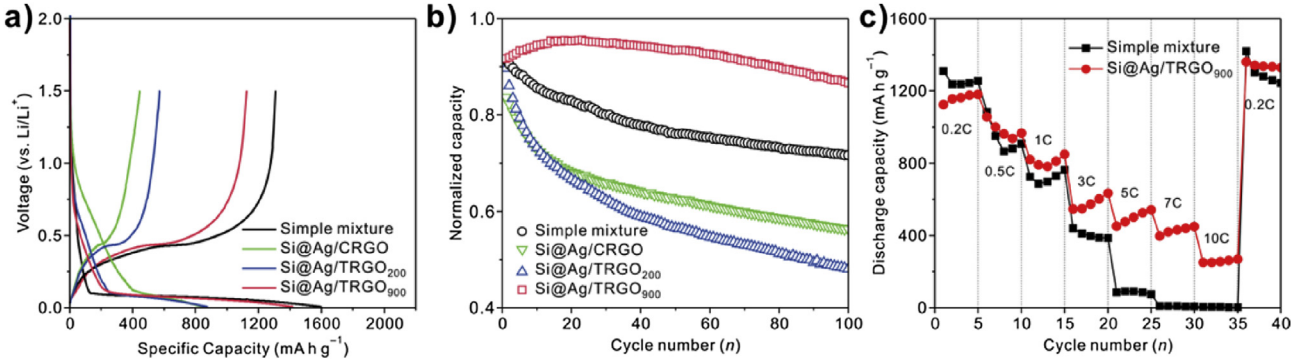

Fig. 3. Electrochemical evaluation of Si@Ag/CRGO, Si@Ag/TRGO fibers and a simple mixture of Si@Ag and TRGO$_{900}$: (a) First cycle and (b) charge capacity normalized cycling performance with different reduction processes. (c) Rate capabilities (0.2–10C) of simple mixture and Si@Ag/TRGO$_{900}$. The first cycle voltage profiles were obtained at 0.05C rate.

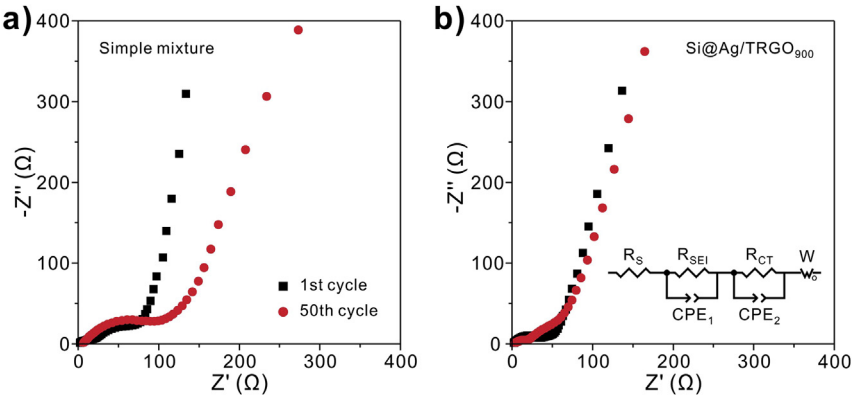

Fig. 4. Electrochemical impedance spectra (EIS) of (a) simple mixture and (b) core/shell structured Si@Ag/$TRGO_{900}$ electrodes after first and 50th cycles. The inset in part b represents the equivalent circuit.

electron transport between active materials. Since the cell does not operate in the absence of conducting agents in Si anode, the incorporation of conducting agent into Si anode materials is essential to overcome its low intrinsic electrical property. Thus, it would be meaningful to investigate cell performance of the electrode without conducting agent in Si anode system. Because $TRGO_{900}$ could provide a high electrical conductivity to Si nanoparticles, it was expected not to require additional conducting agent like super P carbon black.

As such, $TRGO_{900}$ fibers were used as the anode, the first discharge and charge capacities were 503 mA h g^{-1} and 210 mA h g^{-1}, respectively, with a coulombic efficiency of 41.7%.

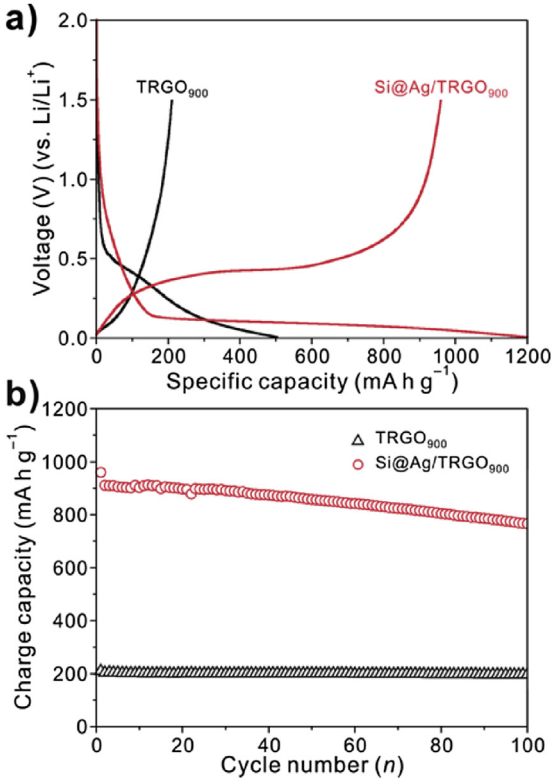

Fig. 5. Electrochemical evaluation of Si@Ag/$TRGO_{900}$ electrode prepared without a conducting agent. (a) First cycle voltage profiles of $TRGO_{900}$ and Si@Ag/$TRGO_{900}$ electrodes were obtained at 0.05C rate in the voltage ranges of 0.005–1.5 V. (b) Cycling performances of $TRGO_{900}$ and Si@Ag/$TRGO_{900}$ electrodes obtained at the same voltage range at 0.2C rate.

After 100 cycles at 0.2C rate, the charge capacity was 196 mA h g^{-1}, corresponding to the capacity retention of 93.3% compared to the first cycle. In addition, the Si@Ag/$TRGO_{900}$ electrode without a conducting agent showed discharge and charge capacities of 1204 mA h g^{-1} and 960 mA h g^{-1}, respectively, with a coulombic efficiency of 79.7% and the charge capacity was 766 mA h g^{-1} after 100 cycles, corresponding to the capacity retention of 79.8%. The charge capacity of Si@Ag with conducting agent after 100 cycles at 0.2C rate was 1320 mA h g^{-1} with the first charge capacity of 1550 mA h g^{-1}; however without a conducting agent, it exhibited severe deterioration of cycling performance [30]. Although the specific capacity of Si@Ag/$TRGO_{900}$ without any other conducting agent was slightly lower than that of the Si@Ag and Si@Ag/$TRGO_{900}$ electrode with the conducting agent, it showed relatively good cycling retention, because $TRGO_{900}$ that provides an electrical pathway could compensate for the lower electrical conductivity of the Si nanoparticles. This result suggests that the double locked Si@Ag/$TRGO_{900}$ fiber electrode fabricated by wet-spinning exhibits enough electrical conductivity even in the absence of conducting agents leading to significantly improved electrochemical performances, including high specific capacity, stable cycling, and high rate capabilities.

4. Conclusion

We presented a facile process based on wet spinning to fabricate graphene-enveloped Si@Ag fibers with a core/shell structure. After additional chemical and thermal reduction, the graphene sheets were found to have fewer structural defects with a significant enhancement in the electrical conductivity. This treatment led to improved electrochemical performances, including a high reversible capacity, stable cycling retention, and superior rate capabilities in LIBs. In addition, the double locked Ag-coated Si-graphene core/shell structure not only alleviated large volume change, but also markedly improved the electrical conductivity of Si nanoparticles. Furthermore, we demonstrated that Si@Ag/$TRGO_{900}$ can be used without the addition of conducting agents. This simple and versatile method can be extended to other nanoparticles to synthesize high-performance anode materials for practical rechargeable-battery applications.

Acknowledgments

This research was supported by the Development Program of the Korea Institute of Energy Research (KIER) (B4-2424) and by the National Research Foundation of Korea (NRF) grant (NRF-

2014R1A2A1A11052829 and 2015–01003143). M. Gu acknowledges financial support from the Global Ph.D. Fellowship (GPF) funded by National Research Foundation of Korea (NRF) (NRF-2013H1A2A1033278).

Appendix A. Supplementary data

Supplementary data related to this article can be found at http://dx.doi.org/10.1016/j.jpowsour.2015.09.083.

References

[1] J.M. Tarascon, M. Armand, Nature 414 (2001) 359–367.
[2] P.G. Bruce, B. Scrosati, J.-M. Tarascon, Angew. Chem. Int. Ed. 47 (2008) 2930–2946.
[3] A. Magasinski, P. Dixon, B. Hertzberg, A. Kvit, J. Ayala, G. Yushin, Nat. Mater 9 (2010) 353–358.
[4] H. Wu, Y. Cui, Nano Today 7 (2012) 414–429.
[5] B.M. Bang, H. Kim, H.-K. Song, J. Cho, S. Park, Energy Environ. Sci. 4 (2011) 5013–5019.
[6] M.N. Obrovac, L.J. Krause, J. Electrochem. Soc. 154 (2007) A103–A108.
[7] N.-S. Choi, Z. Chen, S.A. Freunberger, X. Ji, Y.-K. Sun, K. Amine, G. Yushin, L.F. Nazar, J. Cho, P.G. Bruce, Angew. Chem. Int. Ed. 51 (2012) 9994–10024.
[8] J.R. Szczech, S. Jin, Energy Environ. Sci. 4 (2011) 56–72.
[9] X. Su, Q. Wu, J. Li, X. Xiao, A. Lott, W. Lu, B.W. Sheldon, J. Wu, Adv. Energy Mater 4 (2014).
[10] S. Goriparti, E. Miele, F. De Angelis, E. Di Fabrizio, R.P. Zaccaria, C. Capiglia, J. Power Sources 257 (2014) 421–443.
[11] H. Wu, G. Chan, J.W. Choi, I. Ryu, Y. Yao, M.T. McDowell, S.W. Lee, A. Jackson, Y. Yang, L. Hu, Y. Cui, Nat. Nanotechnol. 7 (2012) 309–314.
[12] S. Xin, Y.-G. Guo, L.-J. Wan, Acc. Chem. Res. 45 (2012) 1759–1769.
[13] M.L. Terranova, S. Orlanducci, E. Tamburri, V. Guglielmotti, M. Rossi, J. Power Sources 246 (2014) 167–177.
[14] X. Zhou, Y.-X. Yin, L.-J. Wan, Y.-G. Guo, Adv. Energy Mater. 2 (2012) 1086–1090.
[15] R. Yi, J. Zai, F. Dai, M.L. Gordin, D. Wang, Nano Energy 6 (2014) 211–218.
[16] M. Zhou, F. Pu, Z. Wang, T. Cai, H. Chen, H. Zhang, S. Guan, Phys. Chem. Chem. Phys. 15 (2013) 11394–11401.
[17] X. Zhou, Y.-X. Yin, L.-J. Wan, Y.-G. Guo, Chem. Comm. 48 (2012) 2198–2200.
[18] S.E. Lee, H.-J. Kim, H. Kim, J.H. Park, D.-G. Choi, Nanoscale 5 (2013) 8986–8991.
[19] F. Sun, K. Huang, X. Qi, T. Gao, Y. Liu, X. Zou, X. Wei, J. Zhong, Nanoscale 5 (2013) 8586–8592.
[20] J.K. Lee, K.B. Smith, C.M. Hayner, H.H. Kung, Chem. Comm. 46 (2010) 2025–2027.
[21] Y.-S. He, P. Gao, J. Chen, X. Yang, X.-Z. Liao, J. Yang, Z.-F. Ma, RSC Adv. 1 (2011) 958–960.
[22] C. Sun, Y. Deng, L. Wan, X. Qin, G. Chen, ACS Appl. Mater. Interfaces 6 (2014) 11277–11285.
[23] Y. Wen, Y. Zhu, A. Langrock, A. Manivannan, S.H. Ehrman, C. Wang, Small 9 (2013) 2810–2816.
[24] R. Hu, W. Sun, Y. Chen, M. Zeng, M. Zhu, J. Mater. Chem. A 2 (2014) 9118–9125.
[25] W. Sun, R. Hu, H. Liu, M. Zeng, L. Yang, H. Wang, M. Zhu, J. Power Sources 268 (2014) 610–618.
[26] Z.-L. Xu, B. Zhang, J.-K. Kim, Nano Energy 6 (2014) 27–35.
[27] X. Zhou, Y.-G. Guo, J. Mater. Chem. A 1 (2013) 9019–9023.
[28] J. Chang, X. Huang, G. Zhou, S. Cui, P.B. Hallac, J. Jiang, P.T. Hurley, J. Chen, Adv. Mater 26 (2014) 758–764.
[29] L. Ji, H. Zheng, A. Ismach, Z. Tan, S. Xun, E. Lin, V. Battaglia, V. Srinivasan, Y. Zhang, Nano Energy 1 (2012) 164–171.
[30] S. Yoo, J.-I. Lee, S. Ko, S. Park, Nano Energy 2 (2013) 1271–1278.
[31] W.S. Hummers, R.E. Offeman, J. Am. Chem. Soc. 80 (1958), 1339–1339.
[32] T.-K. Hong, D.W. Lee, H.J. Choi, H.S. Shin, B.-S. Kim, ACS Nano 4 (2010) 3861–3868.
[33] J. Zou, F. Kim, ACS Nano 6 (2012) 10606–10613.
[34] H. Xiang, K. Zhang, G. Ji, J.Y. Lee, C. Zou, X. Chen, J. Wu, Carbon 49 (2011) 1787–1796.
[35] S.-M. Paek, E. Yoo, I. Honma, Nano Lett. 9 (2009) 72–75.
[36] R. Fong, U. Vonsacken, J.R. Dahn, J. Electrochem. Soc. 137 (1990) 2009–2013.
[37] P. Lian, X. Zhu, S. Liang, Z. Li, W. Yang, H. Wang, Electrochim. Acta 55 (2010) 3909–3914.
[38] D. Aurbach, J. Power Sources 89 (2000) 206–218.